A Deterministic Attitude Estimation Using A Single Vector Information and Rate Gyros

Abraham P. Vinod, Arun D. Mahindrakar, *Member, IEEE*,
Sandipan Bandyopadhyay and
Vijay Muralidharan, *Student Member, IEEE*.

***Abstract*—This paper proposes a deterministic estimator for the estimation of the attitude of a rigid body. A deterministic estimator uses a minimal set of information and does not try to minimize a cost function or fit the measurements into a stochastic process. The proposed estimator obtains the attitude estimation utilizing only the properties of the rotational group $SO(3)$. The information set required by the proposed estimator is a single vector information and rate gyro readings. For systems in which one of the rotational freedom is constrained, the proposed estimator provides an accurate estimate of the reduced attitude. The performance of the algorithm is verified on different experimental testbeds.**

***Index Terms*—Attitude estimation, Inertial Measurement Unit, Special Orthogonal Group, Deterministic algorithm**

I. Introduction

The rotation matrix is an elegant means to capture the transformation between two coordinate frames, irrespective of the relative motion of the frames. The linear transformation helps in determining and explaining several key phenomena seen while studying coordinate frames undergoing relative motion. It plays a key role in the study of kinematics and robotics as can be seen in [1]. Rotation matrices also help in solving the problem of attitude control, e.g, see [2]. The attitude estimation of rigid bodies is a problem that has been explored quite deeply in the past few decades [3]. Attitude estimation for robots [4] and UAVs [5] have, particularly, gained focus in the recent years.

As described in [6], attitude estimation techniques can be classified into two groups - "deterministic" and "optimal". The deterministic estimators use a minimal set of measurements and estimate attitude algebraically by solving a set of simultaneous equations at every step. In scenarios where more information is available, suitable constraints are proposed. Deterministic estimators have minimal dependence on the measurements taken in the previous iteration. Owing to their algebraic constructs, deterministic algorithms are computationally cheaper, but have lesser immunity against measurement noise as compared to optimal estimators [7]. Optimal estimators, on the other hand, try to minimize a cost function, e.g. Wahba's Problem [8], using a larger set of measurements. Several optimal estimators have been proposed based on Kalman filters and complementary filters [3]. Nonlinear complementary filter on the special orthogonal group, proposed by Mahony *et. al* [9], is a popular optimal estimator. The passive complementary filter, proposed in [9], improves a measured estimate of attitude using gyroscope measurements. Detailed research has also been pursued in attitude estimation using using visual-aids [5] and quaternions [10].

Abraham P. Vinod, Arun D. Mahindrakar and Vijay Muralidharan are with the Department of Electrical Engineering, Indian Institute of Technology Madras, Chennai-600036, India, (email: aby.vinod@gmail.com, arun_dm@iitm.ac.in and m_vijay_india@yahoo.co.in),

Sandipan Bandyopadhyay is with the Department of Engineering Design, Indian Institute of Technology Madras, Chennai-600036, India, (email: sandipan@iitm.ac.in).

© 2015 IEEE. Personal use of this material is permitted. Permission from IEEE must be obtained for all other uses, in any current or future media, including reprinting/republishing this material for advertising or promotional purposes, creating new collective works, for resale or redistribution to servers or lists, or reuse of any copyrighted component of this work in other works.

Digital Object Indentifier: 10.1109/TMECH.2015.2404343

Deterministic attitude determination algorithms are used as the measured estimate of attitude for optimal algorithms and in applications that have computational constraints hindering the implementation of optimal algorithms. The TRIAD or the bi-vector method utilizes two vector informations with the constraint that the vectors are mutually orthogonal [11]. Direction Cosine Matrix algorithm tries to fuse the information provided by the popular nine degree-of-freedom (DOF) Inertial Measurement Unit (IMU) to estimate the pose of a rigid body [12].

In this paper, we focus on ground-based robots subjected to low body-accelerations. Owing to their close proximity to magnetic disturbances, attitude estimation using algorithms which utilize magnetometer readings are prone to biases. Hence, we are left with a vector of accelerometer measurements and a vector of rate gyros, which constitute the input to the algorithm developed in this paper. The approach to generalize the algorithm to use any vector measurement measuring a constant vector in the inertial frame and rate gyros is also presented.

We articulate the contributions of this paper as follows. We present a deterministic and numerically stable algorithm for the 3D attitude estimation of a rigid body. The estimate is valid globally on $SO(3)$ and does not require system-based tuning of parameters. The estimator also gives an accurate reduced attitude information for systems with constraints on its rotational freedom. The effect of various sources of error on the attitude estimation is analyzed. Experiments are conducted on two systems: a twin-rotor MIMO system (TRMS) and spherical robot. Experiments validate:
1) the reliability of the 3D attitude estimation algorithm,
2) the coverage of $SO(3)$ with multiple rotations due to the rolling of the spherical robot, and
3) the reduced attitude estimation on TRMS system.

The paper is organized into six sections. In Section II, we discuss the definitions and notations used in the paper. In Section III, we propose the attitude estimator followed by error analysis and discussions in Section IV. The experimental results is presented in Section V with conclusions in Section VI.

II. Definitions and Notations

We follow the definitions given in [1]. Let $||\cdot||$ denote the 2-norm on $\mathbb{R}^n$. The unit sphere in $\mathbb{R}^n$ is defined as $S^{n-1} = \{\boldsymbol{x} \in \mathbb{R}^n : ||\boldsymbol{x}|| = 1\}$. Let $\boldsymbol{I}_3$ denote the 3×3 identity matrix and the orientation of a rigid body be denoted by $\boldsymbol{R}(t) \in SO(3)$ relative to the reference inertial frame, where $SO(3) \triangleq \{\boldsymbol{A} \in \mathbb{R}^{3\times3} : \boldsymbol{A}^\top\boldsymbol{A} = \boldsymbol{I}_3, \det(\boldsymbol{A}) = 1\}$ and $\dot{\boldsymbol{R}}(t) \in T_{\boldsymbol{R}}SO(3)$, the tangent space to $SO(3)$ at $\boldsymbol{R}$. $\{\mathbb{F}\}$ denotes an orthogonal coordinate frame and $\boldsymbol{R}_{F_2}^{F_1}$ maps vectors in $\{\mathbb{F}_2\}$ to $\{\mathbb{F}_1\}$. Since $SO(3)$ is a Lie group, $T_{\boldsymbol{I}}SO(3) \simeq \mathfrak{so}(3)$ acts as Lie algebra of the group, where $\boldsymbol{I}_3$ is the identity element of the group $SO(3)$, $\mathfrak{so}(3)$ is a vector space formed by 3×3 skew-symmetric matrices. Since $\mathfrak{so}(3)$ is isomorphic to $\mathbb{R}^3$, the wedge operator '$\wedge$' is defined such that $\boldsymbol{x} = \{x_1, x_2, x_3\} \in \mathbb{R}^3 \mapsto \widehat{\boldsymbol{x}} \in \mathfrak{so}(3)$ and '$\vee$', the vee operator is defined as the inverse of the wedge operation, that is, $(\hat{\boldsymbol{\omega}})^\vee = \boldsymbol{\omega}$.

We represent $\boldsymbol{R}$ as $\boldsymbol{R} \triangleq \begin{bmatrix} \boldsymbol{c}_1 & \boldsymbol{c}_2 & \boldsymbol{c}_3 \end{bmatrix} \triangleq \begin{bmatrix} \boldsymbol{r}_1 & \boldsymbol{r}_2 & \boldsymbol{r}_3 \end{bmatrix}^\top$ where the columns $(\boldsymbol{c}_1, \boldsymbol{c}_2, \boldsymbol{c}_3)$ and the rows $(\boldsymbol{r}_1, \boldsymbol{r}_2, \boldsymbol{r}_3)$ are mutually orthogonal vectors in S^2. The body angular velocity, $\boldsymbol{\omega} \in \mathbb{R}^3$, associated with a rotation matrix is given by the relation $\boldsymbol{\omega} = (\boldsymbol{R}^\top\dot{\boldsymbol{R}})^\vee$. Similarly, the spatial angular velocity, $\boldsymbol{\Omega} \in \mathbb{R}^3$, is defined as $\boldsymbol{\Omega} = (\dot{\boldsymbol{R}}\boldsymbol{R}^\top)^\vee$.

Euler angle representation uses three angles to represent a unique orientation in $SO(3)$. The angle definitions depend on the chosen axis representation. Since $SO(3)$ is a 3-dimensional manifold, $\boldsymbol{R}$ can not be globally described using a single Euler angle representation.

Given any vector $\boldsymbol{p} \in S^2$, we define a vector correspondence as the pair of vector resolutions of $\boldsymbol{p}$ in two distinct coordinate frames. In this paper, we use the body coordinate frame and the inertial frame when discussing vector correspondences.

III. Deterministic attitude estimation using single vector information and rate gyros - DAESR

Let $\boldsymbol{R}_{\boldsymbol{\eta}}(\theta)$ denote a rotation of $\theta \in S^1$ about $\boldsymbol{\eta} \in S^2$ as given by Euler's axis-angle theorem [1]. Rodrigues' formula, as demonstrated by Piovan and Bullo in [13], helps in obtaining $\boldsymbol{R}_{\boldsymbol{v}\to\boldsymbol{v}_e}$ that maps any two vectors $\boldsymbol{v}, \boldsymbol{v}_e \in S^2$ by the relation $\boldsymbol{v}_e = \boldsymbol{R}_{\boldsymbol{v}\to\boldsymbol{v}_e}\boldsymbol{v}$. The work also provides a general decomposition of a rotation matrix linking two vectors. The general rotation matrix linking two vectors $\boldsymbol{v}, \boldsymbol{v}_e \in S^2$ can be written down as product of two rotations, given by $\boldsymbol{R} = \exp(\alpha\widehat{\boldsymbol{v}}_e)\exp(\theta\widehat{\boldsymbol{\eta}}) = \boldsymbol{R}_{\boldsymbol{v}_e}(\alpha)\boldsymbol{R}_{\boldsymbol{\eta}}(\theta)$. Here, $\alpha \in S^1$ and $\boldsymbol{\eta}, \theta$ are provided by the Rodrigues' formula linking $\boldsymbol{v}$ to $\boldsymbol{v}_e$ whenever $\boldsymbol{v} \times \boldsymbol{v}_e \neq 0$. When $\boldsymbol{v} \times \boldsymbol{v}_e = 0$, we only know $\boldsymbol{\eta} \perp \boldsymbol{v}_e$.

We define the attitude estimation problem, for this paper, as determining the orientation of a rigid body from a single vector correspondence and rate gyro readings. In particular, we choose a vector correspondence such that the resolution of a vector $\boldsymbol{v} \in S^2$, measured in the body frame, is a vector $\boldsymbol{v}_e \in S^2$ constant in the inertial frame. In other words, the attitude estimation problem involves finding $\boldsymbol{R}_{\text{est}} \in SO(3)$ such that $\boldsymbol{v}_e = \boldsymbol{R}_{\text{est}}\boldsymbol{v}$ and $\boldsymbol{R}_{\text{est}}^\top\dot{\boldsymbol{R}}_{\text{est}} = \boldsymbol{\omega}$ with $\boldsymbol{v}_e$ defined as a constant vector in the inertial frame. We assume the following:

1) The body coordinate frame of interest $\{\mathbb{B}\}$ is related to the measuring device coordinate frame $\{\mathbb{G}\}$ by the rotation matrix $\boldsymbol{R}_B^G \triangleq \boldsymbol{R}_B$. Since the measuring device is attached to the body, $\boldsymbol{R}_B$ is constant.

2) An inertial coordinate frame $\{\mathbb{I}\}$ which has one of its axes along the direction of $\boldsymbol{v}_e$ and is rotated about $\boldsymbol{v}_e$ so that $\{\mathbb{I}\}$ coincides with $\{\mathbb{G}\}$ at the start of the experiment. The inertial coordinate frame of interest $\{\mathbb{I}_0\}$ for the estimator is related to the frame $\{\mathbb{I}\}$ by the rotation matrix $\boldsymbol{R}_I^{I_0} \triangleq \boldsymbol{R}_I$. Since $\{\mathbb{I}\}$ and $\{\mathbb{I}_0\}$ are inertial frames, $\boldsymbol{R}_I$ is constant.

3) An intermediary non-inertial coordinate frame $\{\mathbb{I}_1\}$, which is a coordinate frame obtained by rotating $\{\mathbb{I}\}$ about $\boldsymbol{v}_e$ by α. Hence, $\boldsymbol{R}_{I_1}^I \triangleq \boldsymbol{R}_{\boldsymbol{v}_e}(\alpha)$. At the start of the experiment, $\alpha = 0$ causing $\{\mathbb{I}_1\}$ to coincide with $\{\mathbb{I}\}$ and $\{\mathbb{G}\}$.

Accelerometers provide earth's gravity vector measurement accurately only when system is at rest or is undergoing a very small acceleration [4]. Therefore, the normalized accelerometer output can be used as a candidate for $\boldsymbol{v}$ in low-dynamic environments. Proposition IV.1 discusses the effect of this assumption on the attitude estimation. We demonstrate in Section V that a robust attitude estimation is obtained when accelerometer based DAESR is used as the measured attitude estimate for a complimentary filter based attitude estimator [9]. We now formulate the framework to assist in the theoretical development of the algorithm.

A. Formulation of attitude estimation problem

Consider the problem of estimating the attitude of a rigid body using accelerometer reading $\boldsymbol{a}$ and rate gyro sensors $\boldsymbol{\omega}$. Since rotation matrix is a norm-preserving linear transformation, $\boldsymbol{a}$ can be approximated to lie in S^2. $\boldsymbol{R}_I$ and $\boldsymbol{R}_B$ are constant matrices known *a priori* and do not appear in the measurements. Hence, we can consider without loss of generality $\boldsymbol{R}_I = \boldsymbol{R}_B = \boldsymbol{I}_3$. We define a framework as $\boldsymbol{v} = -\boldsymbol{a}$, $\boldsymbol{v}_e = \boldsymbol{e}_3$, $\{\mathbb{I}\} = \{\mathbb{I}_0\} = \{\boldsymbol{e}_1, \boldsymbol{e}_2, \boldsymbol{e}_3\}$, $\{\mathbb{I}_1\} = \{\boldsymbol{e}_1^*, \boldsymbol{e}_2^*, \boldsymbol{e}_3^*\}$ and $\{\mathbb{G}\} = \{\mathbb{B}\} = \{\boldsymbol{e}_1', \boldsymbol{e}_2', \boldsymbol{e}_3'\}$. Here,

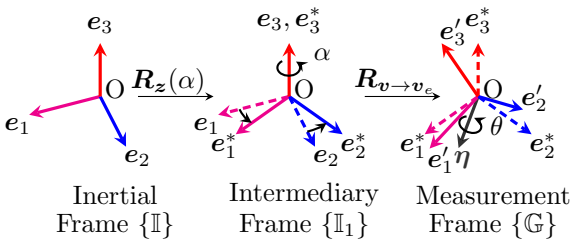

Figure 1: Frames for a typical attitude estimation

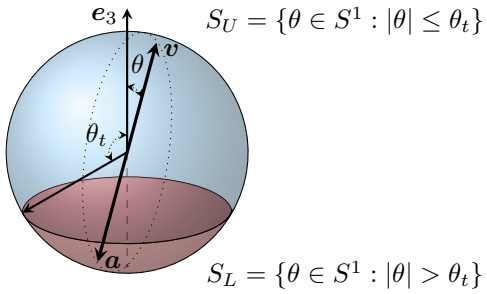

Figure 2: Definitions of θ, θ_t, S_U and S_L for framework given in Subsection III-A

$\boldsymbol{e}_i$, $\boldsymbol{e}_i^*$ and $\boldsymbol{e}_i'$, for $i \in \{1, 2, 3\}$, are standard basis vectors in their corresponding frames. We define $\boldsymbol{R}_{\text{est}} = \boldsymbol{R}_B^{I_0}$ as

$$\boldsymbol{R}_{\text{est}} = \boldsymbol{R}_I^{I_0}\boldsymbol{R}_{I_1}^I\boldsymbol{R}_G^{I_1}\boldsymbol{R}_B^G = \boldsymbol{R}_I\boldsymbol{R}_{I_1}^I\boldsymbol{R}_G^{I_1}\boldsymbol{R}_B = \exp(\alpha\widehat{\boldsymbol{v}}_e)\exp(\theta\widehat{\boldsymbol{\eta}}) = \boldsymbol{R}_{\boldsymbol{v}_e}(\alpha)\boldsymbol{R}_{\boldsymbol{v}\to\boldsymbol{v}_e} \quad (1)$$

where α is the angle of rotation about $\boldsymbol{v}_e$ for aligning $\{\mathbb{I}_1\}$ with $\{\mathbb{I}\}$. Figure 1 captures the transitions undergone during the attitude estimation with $\boldsymbol{R}_I = \boldsymbol{R}_B = \boldsymbol{I}_3$. The DAESR algorithm, for this framework, has been described in Algorithm 1 and notations used in this section and in Algorithm 1 are summarized in Table I.

As seen in (1), DAESR needs to estimate α and $\boldsymbol{R}_{\boldsymbol{v}\to\boldsymbol{v}_e}$ to complete the attitude estimation. We first handle the determination of $\boldsymbol{R}_{\boldsymbol{v}\to\boldsymbol{v}_e}$ in Subsection III-B followed by the estimation of α in Subsection III-C.

B. Determination of $\boldsymbol{R}_{\boldsymbol{v}\to\boldsymbol{v}_e}$

We can try to capture $\boldsymbol{R}_{\boldsymbol{v}\to\boldsymbol{v}_e}$ using the angle-axis form $\boldsymbol{R}_{\boldsymbol{\eta}}(\theta)$. As described in [13], we have $\boldsymbol{\eta} = \frac{\boldsymbol{v}\times\boldsymbol{v}_e}{\|\boldsymbol{v}\times\boldsymbol{v}_e\|}$ which makes $\boldsymbol{R}_{\boldsymbol{\eta}}(\theta)$ indeterminate when $\boldsymbol{v}$ approaches $\pm\boldsymbol{v}_e$. To avoid these potential numerical issues, we revisit a modified estimate for $\boldsymbol{R}_{\boldsymbol{v}\to\boldsymbol{v}_e}$ presented in [14]. For $\boldsymbol{\eta}^* \triangleq \boldsymbol{v} \times \boldsymbol{v}_e$ and $\cos\theta \triangleq \boldsymbol{v}^\top\boldsymbol{v}_e$,

$$\boldsymbol{R}_{\boldsymbol{v}\to\boldsymbol{v}_e} = \boldsymbol{R}_{\boldsymbol{\eta}^*}(\theta) = \boldsymbol{I}_3 + \widehat{\boldsymbol{\eta}}^* + \frac{(\widehat{\boldsymbol{\eta}}^*)^2}{1+\cos\theta}, \ \forall\ \theta \in S^1/\{\pi\}. \quad (2)$$

Clearly, (2) is good estimator for $\boldsymbol{R}_{\boldsymbol{v}\to\boldsymbol{v}_e}$ as long as $1 + \cos\theta$ is not close to 0 or equivalently $\theta \in S_U$ where $S_U = \{\boldsymbol{v} \in S^2 : \theta = \cos^{-1}(\boldsymbol{v}^\top\boldsymbol{v}_e) \in [0, \theta_t]\}$ for some $\theta_t \in (0, \pi)$. The value of θ_t is motivated at the end of this subsection. For $S_L = S^2 \setminus S_U$, θ is close to π or $\boldsymbol{v}$ close to $-\boldsymbol{v}_e$ as seen in Figure 2. Estimation of $\boldsymbol{R}_{\boldsymbol{v}\to\boldsymbol{v}_e}$ when $\theta \in S_L$ can be done using an Euler angle representation which satisfies the following points:

1) Since determining all Euler angles is not feasible from a single vector correspondence, we determine the third Euler angle by ensuring that the choice of the Euler angle representation is such that its rightmost axis is aligned along $\boldsymbol{v}_e$.

2) Euler angle representation, by definition, possesses two singularity

points. The choice of the Euler angle representation and θ_t should allow S_L to be a singularity free set.

For the framework described in Subsection III-A, we choose ZYX sequence of Euler angles (ψ, δ, γ). This allows for the redefinition of $\boldsymbol{R}_{\boldsymbol{v}\to\boldsymbol{v}_e}$ as $\boldsymbol{R}_{\boldsymbol{z}}(\psi)\boldsymbol{R}_{\boldsymbol{y}}(\delta)\boldsymbol{R}_{\boldsymbol{x}}(\gamma)$ where $\boldsymbol{z} = \boldsymbol{e}_3^*, \boldsymbol{y} = \boldsymbol{R}_{\boldsymbol{z}}(\psi)\boldsymbol{e}_2^*$ and $\boldsymbol{x} = \boldsymbol{R}_{\boldsymbol{y}}(\delta)\boldsymbol{R}_{\boldsymbol{z}}(\psi)\boldsymbol{e}_1^*$ when $\theta \in S_L$. By definition of $\boldsymbol{v}_e$, $\boldsymbol{e}_3 = \boldsymbol{e}_3^*$. This Euler angle parameterization is also referred to as yaw (ψ), pitch (δ) and roll (γ) parameterization. Due to the singularity at $\delta = \pm\frac{\pi}{2}$ in the ZYX representation, $|\theta_t| > \frac{\pi}{2}$ to make S_L singularity free.

Using θ_t to partition S^2 into S_U and S_L, we utilize (1), the relation $\boldsymbol{R}_{\boldsymbol{v}_e}(\alpha) = \boldsymbol{R}_{\boldsymbol{z}}(\alpha)$ and the definition of ψ to redefine $\boldsymbol{R}_{\text{est}}$ as follows,

$$\boldsymbol{R}_{\text{est}} = \begin{cases} \boldsymbol{R}_{\boldsymbol{z}}(\alpha)\boldsymbol{R}_{\boldsymbol{v}\to\boldsymbol{v}_e}, & \theta \in S_U \\ \boldsymbol{R}_{\boldsymbol{z}}(\alpha+\psi)\boldsymbol{R}_{\boldsymbol{y}}(\delta)\boldsymbol{R}_{\boldsymbol{x}}(\gamma), & \theta \in S_L. \end{cases} \tag{3}$$

The rotation about $\boldsymbol{v}_e$, $\boldsymbol{R}_{\boldsymbol{z}}(\alpha)$ or $\boldsymbol{R}_{\boldsymbol{z}}(\alpha+\psi)$, is obtained from integrating the rate of rotation about $\boldsymbol{v}_e$. This yields a constant of integration, $\boldsymbol{R}_C$. By construction, $\boldsymbol{R}_C = \boldsymbol{R}_{\boldsymbol{z}}(\beta),\ \beta \in S^1$ and its value changes value only during transitions to account for initial value of ψ. Estimation of the rate of rotation about $\boldsymbol{v}_e$ is deferred for Subsection III-C. We define $\boldsymbol{R}_E = \boldsymbol{R}_{\boldsymbol{y}}(\delta)\boldsymbol{R}_{\boldsymbol{x}}(\gamma)$.

Defining $\boldsymbol{R}_U$ and $\boldsymbol{R}_L$ as $\boldsymbol{R}_{\text{est}}$ for S_U and S_L respectively, we have $\boldsymbol{R}_U = \boldsymbol{R}_{\boldsymbol{z}}(\alpha)\boldsymbol{R}_C\boldsymbol{R}_{\boldsymbol{v}\to\boldsymbol{v}_e}$ and $\boldsymbol{R}_L = \boldsymbol{R}_{\boldsymbol{z}}(\alpha+\psi)\boldsymbol{R}_C\boldsymbol{R}_E$ where α and $(\alpha+\psi)$ now only contains the changes in α and $(\alpha+\psi)$ after the respective transitions. We obtain $\boldsymbol{R}_C$ as

$$\boldsymbol{R}_C = \begin{cases} \boldsymbol{R}_L\boldsymbol{R}_{\boldsymbol{v}\to\boldsymbol{v}_e}^\top, & S_L \to S_U \\ \boldsymbol{R}_U\boldsymbol{R}_E^\top, & S_U \to S_L. \end{cases} \tag{4}$$

The assumption used is that the estimates, $\boldsymbol{R}_U$ and $\boldsymbol{R}_L$, are both reliable in the neighbourhood of the boundary $\theta = \theta_t$. This assumption requires a sufficient margin between θ_t and the singularities of the Euler angle decomposition of $\boldsymbol{R}_{\boldsymbol{v}\to\boldsymbol{v}_e}$. To achieve the margin and a numerically stable estimate of $\frac{1}{1+\cos\theta}$, we choose $\theta_t = \frac{2\pi}{3}$.

We redefine the estimated attitude given by (1) as,

$$\boldsymbol{R}_{\text{est}} = \boldsymbol{R}_I\boldsymbol{R}_A\boldsymbol{R}_C\boldsymbol{R}_V\boldsymbol{R}_B \tag{5}$$

where, $\boldsymbol{R}_I = \boldsymbol{R}_B = \boldsymbol{I}_3$ and $\boldsymbol{R}_A = \boldsymbol{R}_{\boldsymbol{z}}(\alpha_0)$ with

$$\alpha_0 = \begin{cases} \alpha, & \theta \in S_U \\ \alpha+\psi, & \theta \in S_L \end{cases} \text{ and } \boldsymbol{R}_V = \begin{cases} \boldsymbol{R}_{\boldsymbol{v}\to\boldsymbol{v}_e}, & \theta \in S_U \\ \boldsymbol{R}_E, & \theta \in S_L \end{cases}.$$

The estimation starts with $\boldsymbol{R}_C = \boldsymbol{R}_A = \boldsymbol{I}_3$. When $\boldsymbol{v}$ crosses the boundary, we estimate the orientation $\boldsymbol{R}_{\text{est}}$ using the previous set's estimation formula and set $\boldsymbol{R}_A = \boldsymbol{I}_3$ after updating $\boldsymbol{R}_C$ using (4). $\boldsymbol{R}_C$ does not change as long as θ does not cross the boundary $\theta = \theta_t$. The difference between the two cases of the definition of $\boldsymbol{R}_V$ is $\boldsymbol{R}_z(\psi)$. We now look at estimating $\boldsymbol{R}_V$ when $\theta \in S_L$.

Proposition III.1. *Given $\theta \in S_L$ and the normalized accelerometer readings $\boldsymbol{a} = (a_x, a_y, a_z)$,*

$$\boldsymbol{R}_E = \boldsymbol{R}_{\boldsymbol{y}}(\delta)R_{\boldsymbol{x}}(\gamma) = \begin{bmatrix} \sqrt{a_y^2+a_z^2} & -\frac{a_xa_y}{\sqrt{a_y^2+a_z^2}} & -\frac{a_xa_z}{\sqrt{a_y^2+a_z^2}} \\ 0 & -\frac{a_z}{\sqrt{a_y^2+a_z^2}} & \frac{a_y}{\sqrt{a_y^2+a_z^2}} \\ -a_x & -a_y & -a_z \end{bmatrix}$$

Proof: For $\theta \in S_L$, from ZYX Euler angle representation,

$$\boldsymbol{R}_{\boldsymbol{y}}(\delta)\boldsymbol{R}_{\boldsymbol{x}}(\gamma) = \begin{bmatrix} \cos\delta & \sin\gamma\sin\delta & \cos\gamma\sin\delta \\ 0 & \cos\gamma & -\sin\gamma \\ -\sin\delta & \cos\delta\sin\gamma & \cos\gamma\cos\delta \end{bmatrix}.$$

From (5), we can frame the constraint $\boldsymbol{e}_3 = -\boldsymbol{R}_A\boldsymbol{R}_C\boldsymbol{R}_V\boldsymbol{a}$ or $\boldsymbol{e}_3 = -\boldsymbol{R}_E\boldsymbol{a}$ since $\boldsymbol{R}_C^\top\boldsymbol{R}_{\boldsymbol{z}}^\top(\alpha_0)\boldsymbol{e}_3 = \boldsymbol{e}_3$. Therefore,

$$\sin\delta = \pm\, a_x,\ \cos\delta = \pm\,\sqrt{a_y^2+a_z^2}$$

$$\sin\gamma = \mp\,\frac{a_y}{\sqrt{a_y^2+a_z^2}},\ \cos\gamma = \mp\,\frac{a_z}{\sqrt{a_y^2+a_z^2}}$$

On substitution, for $\tau \in \{0, \pi\}$, $\boldsymbol{R}_E$ becomes,

$$\boldsymbol{R}_E = \boldsymbol{R}_{\boldsymbol{z}}(\tau)\begin{bmatrix} \sqrt{a_y^2+a_z^2} & -\frac{a_xa_y}{\sqrt{a_y^2+a_z^2}} & -\frac{a_xa_z}{\sqrt{a_y^2+a_z^2}} \\ 0 & -\frac{a_z}{\sqrt{a_y^2+a_z^2}} & \frac{a_y}{\sqrt{a_y^2+a_z^2}} \\ -a_x & -a_y & -a_z \end{bmatrix}.$$

While using (4), $\boldsymbol{R}_{\boldsymbol{z}}(\tau)$ gets absorbed into $\boldsymbol{R}_C$. ∎

While Shuster in his discussion of deterministic algorithms [7] uses only the modified Rodrigues' formula discussed in Subsection III-B, the approach of splitting the sphere into separate sets, S_U and S_L ensures numerical stability. This has been verified in the experiments described in Section V and is a major contribution of this paper.

C. Determination of the rotation about $\boldsymbol{e}_3$, $\boldsymbol{R}_A$

From (2), $\boldsymbol{R}_{\boldsymbol{v}\to\boldsymbol{v}_e}$ can be geometrically understood as the linear transformation that aligns $\boldsymbol{v}$ to $\boldsymbol{v}_e$ and is differentiable with respect to time. We can also see that $\boldsymbol{R}_{\boldsymbol{z}}(\alpha)$ and $\boldsymbol{R}_E$ is also differentiable with respect to time. Unfortunately, shifting $\boldsymbol{R}_{\boldsymbol{z}}(\psi)$ to $\boldsymbol{R}_A$ introduces discontinuity in $\boldsymbol{R}_V$ and $\boldsymbol{R}_A$ at the boundary $\theta = \theta_t$. Hence, $\boldsymbol{R}_A$ and $\boldsymbol{R}_V$ are differentiable everywhere except at $\theta = \theta_t$.

Consider the spatial angular velocity $\boldsymbol{\Omega}$ of the frame $\{\mathbb{B}\}$ as seen from $\{\mathbb{I}_0\}$ based on the definition given by (5), for $\theta \neq \theta_t$, $\widehat{\boldsymbol{\Omega}} = \dot{\boldsymbol{R}}_{\text{est}}\boldsymbol{R}_{\text{est}}^\top = (\dot{\boldsymbol{R}}_A\boldsymbol{R}_C\boldsymbol{R}_V + \boldsymbol{R}_A\boldsymbol{R}_C\dot{\boldsymbol{R}}_V)\boldsymbol{R}_V^\top\boldsymbol{R}_C^\top\boldsymbol{R}_A^\top = \widehat{\boldsymbol{\Omega}}_A + \boldsymbol{R}_A\boldsymbol{R}_C\widehat{\boldsymbol{\Omega}}_V\boldsymbol{R}_C^\top\boldsymbol{R}_A^\top$. On applying the '$\vee$' operator and substituting $\boldsymbol{\Omega} = \boldsymbol{R}_A\boldsymbol{R}_C\boldsymbol{R}_V\boldsymbol{\omega}$, we get $\boldsymbol{R}_A\boldsymbol{R}_C\boldsymbol{R}_V\boldsymbol{\omega} = \boldsymbol{\Omega}_A + \boldsymbol{R}_A\boldsymbol{R}_C\boldsymbol{\Omega}_V$. The body angular velocity vector $\boldsymbol{\omega}$ is obtained from rate gyro readings. $\boldsymbol{R}_A$ and $\boldsymbol{R}_C$ are rotations about $\boldsymbol{v}_e$ and hence $\boldsymbol{\omega}_A = \boldsymbol{R}_C^\top\boldsymbol{R}_A^\top\boldsymbol{\Omega}_A = \boldsymbol{\Omega}_A$ is a vector along $\boldsymbol{v}_e$. Therefore,

$$\boldsymbol{R}_V\boldsymbol{\omega} = \boldsymbol{\omega}_A + \boldsymbol{\Omega}_V \tag{6}$$

where $\boldsymbol{\Omega}_V = (\dot{\boldsymbol{R}}_V\boldsymbol{R}_V^\top)^\vee$ and $\boldsymbol{\omega}_A = \dot{\alpha}_0\boldsymbol{v}_e = \dot{\alpha}_0\boldsymbol{e}_3$.

We assumed in Subsection III-B that both $\boldsymbol{R}_U$ and $\boldsymbol{R}_L$ are reliable in the neighbourhood of $\theta = \theta_t$. This assumption, validated in Subsection V-B, allows the definition of $\boldsymbol{\omega}_A$ by (6) to hold true even at $\theta = \theta_t$. The absence of $\boldsymbol{R}_A$ in (6) shows that the given input set can not provide $\boldsymbol{R}_{\text{est}}$ without integration. The integration step is done using the Euler method. Other methods of integration can be explored for better accuracy [15].

D. Estimation of the angular velocity of $\{\mathbb{G}\}$ as seen from $\{\mathbb{I}_1\}$, $\boldsymbol{\Omega}_V$

Equation (6) requires the estimate of $\boldsymbol{\Omega}_V$. Since $\boldsymbol{R}_V$ is differentiable everywhere except at the boundary, $\boldsymbol{\Omega}_V$ will be a smooth function with discontinuities at the boundary. For the framework defined in Subsection III-A, $\boldsymbol{r}_3 = -\boldsymbol{a}$. Shuster discusses the derivative of the attitude in [16] and gives the relation $\dot{\boldsymbol{r}}_i = \boldsymbol{\omega} \times \boldsymbol{r}_i$. Since $\boldsymbol{R}_V = [\boldsymbol{r}_1\ \boldsymbol{r}_2\ \boldsymbol{r}_3]^\top$ is known, we determine $\boldsymbol{e}_1^\top\boldsymbol{\Omega}_V$ and $\boldsymbol{e}_2^\top\boldsymbol{\Omega}_V$ as $\boldsymbol{e}_1^\top\boldsymbol{\Omega}_V = \dot{\boldsymbol{r}}_3^\top\boldsymbol{r}_2$ and $\boldsymbol{e}_2^\top\boldsymbol{\Omega}_V = -\dot{\boldsymbol{r}}_3^\top\boldsymbol{r}_1$.

On the other hand, the determination of $\boldsymbol{e}_3^\top\boldsymbol{\Omega}_V$ requires the time-derivative of the estimates of $\boldsymbol{r}_1$ or $\boldsymbol{r}_2$ which will not be accurate. We note that $\boldsymbol{e}_3^\top\boldsymbol{\Omega}_V$ can be obtained from the simplification of the expression $\boldsymbol{e}_3^\top\boldsymbol{\Omega}_V = \dot{\boldsymbol{r}}_2^\top\boldsymbol{r}_1$,

$$\boldsymbol{e}_3^\top\boldsymbol{\Omega}_V = \begin{cases} \frac{a_x\dot{a}_y - a_y\dot{a}_x}{1-a_z}, & \theta \in S_U \\ \frac{a_x(a_y\dot{a}_z - a_z\dot{a}_y)}{1-a_x^2}, & \theta \in S_L. \end{cases} \tag{7}$$

Figure 2 shows that $-1 \leq a_z \leq 0.5$ in S_U and $|a_x| \leq \frac{\sqrt{3}}{2}$ in S_L due to the choice of $\theta_t = \frac{2\pi}{3}$. The knowledge of $\boldsymbol{\Omega}_V$, and thereby $\boldsymbol{R}_A$, completes the accelerometer based DAESR as given in (5).

We pause here to note that, in a general setting, determination of $\boldsymbol{\omega}_A$ requires the knowledge of $\boldsymbol{\Omega}_V$ along the inertial frame axis

$\boldsymbol{R}_{\text{est}}$- Estimated attitude using DAESR algorithm	
$\boldsymbol{R}_I$ - Rotation from $\{\mathbb{I}_0\}$ to $\{\mathbb{I}\}$	$\boldsymbol{R}_B$ - Rotation from $\{\mathbb{G}\}$ to $\{\mathbb{B}\}$
$\boldsymbol{R}_A$ - Rotation about $\boldsymbol{e}_3$ (5)	$\boldsymbol{R}_L$ - $\boldsymbol{R}_{\text{est}}$ for $\theta \in S_L$
$\boldsymbol{R}_E$ - Rotation using δ and γ	$\boldsymbol{R}_U$ - $\boldsymbol{R}_{\text{est}}$ for $\theta \in S_U$
$\boldsymbol{R}_C$ - Integration constant while integrating $\boldsymbol{\omega}_A$ (4)	$\boldsymbol{R}_{\boldsymbol{\eta}}(\theta)$ - Rotation about $\boldsymbol{\eta}$ as axis and θ as rotation angle
$\boldsymbol{R}_V$ - Rotation satisfying $\boldsymbol{v}_e = R_V \boldsymbol{v}$ using only $\boldsymbol{v}$ information (5)	$\boldsymbol{R}_{\boldsymbol{v}\to\boldsymbol{v}_e}$ - Rotation satisfying $\boldsymbol{v}_e = R_{\boldsymbol{v}\to\boldsymbol{v}_e}\boldsymbol{v}$ using (2)

Table I: Definitions of the variables used in this paper

assigned to $\boldsymbol{v}_e$ and inclusion of $\boldsymbol{R}_I$ and $\boldsymbol{R}_B$ in (5). The choice of Euler angle representation and Proposition III.1 should be suitably modified. We have used a minimal three parameter representation for $\boldsymbol{R}_{\text{est}}$ in DAESR. When $\theta \in S_U$, $\boldsymbol{R}_{\text{est}}$ is represented by $\boldsymbol{\eta}, \theta$ and α_0 with $\boldsymbol{\eta}.\boldsymbol{v}_e = 0$ and $\boldsymbol{\eta} \in S^2$ and when $\theta \in S_L$, γ, δ and α_0 represent $\boldsymbol{R}_{\text{est}}$.

E. Reduced attitude estimate from DAESR

Some of the dynamical systems have constrained degrees of rotational freedom. For example, mobile inverted pendulum moving in a horizontal plane does not have roll dynamics [17]. For systems which have dormant roll-dynamics ($\gamma = 0$), using the framework specified in Subsection III-A, $\boldsymbol{a}$ is constrained in the coordinate plane $x - z$ corresponding to $\{\mathbb{G}\}$. Hence, $\boldsymbol{R}_{\boldsymbol{z}}(\psi) = \boldsymbol{I}_3$. This relation is true even if pitch is the constrained DOF instead of roll. For such systems, α_0, defined in (5), becomes yaw and the estimator gives an accurate reduced attitude description of the body [18]. Since $\psi = 0$, $\boldsymbol{R}_{\boldsymbol{v}\to\boldsymbol{v}_e} = \boldsymbol{R}_E$. On the other hand, if yaw is the constrained DOF, then the reduced attitude estimate coincides with the complete attitude estimate since $\dot{\alpha}_0 = 0$. Generalizing from this discussion, we can say for systems which have at least one constrained degree of rotational freedom, DAESR provides an accurate estimate of the reduced attitude. In a general setting, α_0 is not equal to any of the Euler angles as seen in Subsection III-B.

Next, we will analyze various sources of error and their influence on the estimator followed by the experimental validation.

IV. Analysis of various sources of error in the estimate

The major sources of error in DAESR are due to the bias in rate gyro readings and the errors in the estimates of $\boldsymbol{v}$, $\dot{\boldsymbol{v}}$ and α_0. In this section, the measured quantities will be denoted by $\tilde{x}$ to distinguish from their theoretical counterparts x. We define $\Delta x = \tilde{x} - x$.

A. Error due to rate gyros

The noise present in the rate gyro readings are due to Angular Random Walk (ARW), gyroscopic drift and measurement noise [19]. We assume a simple constant bias model for the error in the rate gyro readings which is determined by averaging the rate gyro readings during the time in which the rigid body was motionless. From Subsection III-B, it is clear that $\boldsymbol{\omega}$ only influences the estimates of $\boldsymbol{R}_A$ and $\boldsymbol{R}_C$. When considering a noisy rate gyro, (6) becomes $\boldsymbol{\omega}_A = \boldsymbol{R}_V \boldsymbol{R}_B\ (\boldsymbol{\omega} + \Delta\boldsymbol{\omega}) - \boldsymbol{\Omega}_V$. Let $\boldsymbol{R}^*_{AC}$ correspond to the rotation about $\boldsymbol{e}_3$ by an angle equivalent to the time integral of $\boldsymbol{e}_3^\top(\boldsymbol{R}_V \boldsymbol{R}_B \Delta\boldsymbol{\omega})$. On integrating the erroneous $\dot{\alpha}_0$, $\boldsymbol{R}_A\boldsymbol{R}_C$ becomes $\boldsymbol{R}_A\boldsymbol{R}_C\boldsymbol{R}^*_{AC}$ and the error in $\boldsymbol{R}_{\text{est}}$ manifests as $\boldsymbol{R}_{\text{est}}\boldsymbol{R}^*_{\text{est}}$ where $\boldsymbol{R}^*_{\text{est}} = \boldsymbol{R}_B^\top \boldsymbol{R}_V^\top \boldsymbol{R}^*_{AC} \boldsymbol{R}_V \boldsymbol{R}_B$. For $\frac{||\Delta\boldsymbol{\omega}||}{||\boldsymbol{\omega}||} \ll 1$, $\boldsymbol{R}^*_{AC}$ approaches $\boldsymbol{I}_3$.

B. Error in the estimate of $\boldsymbol{v}$

The measurement of vector $\boldsymbol{v}$ could have errors introduced by sensing. Equation (5) can be modified as $\tilde{\boldsymbol{R}}_{\text{est}} = \boldsymbol{R}_I \boldsymbol{R}_A \boldsymbol{R}_C \boldsymbol{R}_V \boldsymbol{R}_{\tilde{\boldsymbol{v}}\to\boldsymbol{v}} \boldsymbol{R}_B$.

Algorithm 1 Description of DAESR (Table I lists the used variables)

Input: $\boldsymbol{R}_I$, $\boldsymbol{R}_B$, accelerometer ($\boldsymbol{a}, \boldsymbol{a}_{\text{prev}}$) and rate gyro ($\boldsymbol{\omega}$) readings, $\theta_t = \frac{2\pi}{3}$, $\boldsymbol{R}_C = \boldsymbol{I}_3$, $\alpha_0 = 0$. $\boldsymbol{R}_C, \alpha_0$ are constantly fed back.

Output: $[\boldsymbol{R}_{\text{est}}, \boldsymbol{R}_C, \alpha_0]$

procedure DAESR($\boldsymbol{a}, \boldsymbol{a}_{\text{prev}}, \boldsymbol{\omega}, \boldsymbol{R}_C, \alpha_0$)
  $\cos\theta \leftarrow -\boldsymbol{e}_3^\top \boldsymbol{a}$
  $\cos\theta_{\text{prev}} \leftarrow -\boldsymbol{e}_3^\top \boldsymbol{a}_{\text{prev}}$
  $\dot{\boldsymbol{a}} \leftarrow \boldsymbol{\omega} \times \boldsymbol{a}$ ▷ From Subsection III-D
  if $\cos\theta \geq \cos\theta_t$ **then** ▷ $\theta \in S_U$
    Set $\boldsymbol{R}_V$ *as* $\boldsymbol{R}_{\boldsymbol{v}\to\boldsymbol{v}_e}$ *from* (2)
    Obtain $\boldsymbol{e}_3^\top \boldsymbol{\Omega}_V$ *from* (7) *with* $\theta \in S_U$ *using* $\boldsymbol{a}$ *and* $\dot{\boldsymbol{a}}$
    if $\cos\theta_{\text{prev}} \leq \cos\theta_t$ **then** ▷ $S_L \to S_U$
      Use (5) *to get* $\boldsymbol{R}_{est}$ *from* $\boldsymbol{R}_V, \boldsymbol{R}_{\boldsymbol{z}}(\alpha_0), \boldsymbol{R}_I, \boldsymbol{R}_C$ *and* $\boldsymbol{R}_B$ *where* $\boldsymbol{R}_V$ *is* $\boldsymbol{R}_E$ *from Proposition III.1 and* α_0 *is found by integrating* $\boldsymbol{e}_3^\top \boldsymbol{\omega}_A$ *determined from* (6) *and* (7) *using* $\theta \in S_L$
      Update $\boldsymbol{R}_C$ *using* (4) *and set* α_0 *to zero*
      return $[\boldsymbol{R}_{\text{est}}, \boldsymbol{R}_C, \alpha_0]$
    end if
  else ▷ $\theta \in S_L$
    Set $\boldsymbol{R}_V$ *as* $\boldsymbol{R}_E$ *from Proposition III.1*
    Obtain $\boldsymbol{e}_3^\top \boldsymbol{\Omega}_V$ *from* (7) *with* $\theta \in S_L$ *using* $\boldsymbol{a}$ *and* $\dot{\boldsymbol{a}}$
    if $\cos\theta_{\text{prev}} \geq \cos\theta_t$ **then** ▷ $S_U \to S_L$
      Use (5) *to get* $\boldsymbol{R}_{est}$ *from* $\boldsymbol{R}_V, \boldsymbol{R}_{\boldsymbol{z}}(\alpha_0), \boldsymbol{R}_I, \boldsymbol{R}_C$ *and* $\boldsymbol{R}_B$ *where* $\boldsymbol{R}_V$ *is* $\boldsymbol{R}_{\boldsymbol{v}\to\boldsymbol{v}_e}$ *from* (2) *and* α_0 *is found by integrating* $\boldsymbol{e}_3^\top \boldsymbol{\omega}_A$ *determined from* (6) *and* (7) *using* $\theta \in S_U$
      Update $\boldsymbol{R}_C$ *using* (4) *and set* α_0 *to zero*
      return $[\boldsymbol{R}_{\text{est}}, \boldsymbol{R}_C, \alpha_0]$
    end if
  end if
  Handling the case $\{\theta, \theta_{prev}\} \in S_L \times S_L$ ***or*** $S_U \times S_U$
  Use (5) *to get* $\boldsymbol{R}_{est}$ *from* $\boldsymbol{R}_V, \boldsymbol{R}_{\boldsymbol{z}}(\alpha_0), \boldsymbol{R}_I, \boldsymbol{R}_C$ *and* $\boldsymbol{R}_B$ *where* $\boldsymbol{R}_V$ *and* $\boldsymbol{e}_3^\top \boldsymbol{\Omega}_V$ *are already defined and* α_0 *is found by integrating* $\boldsymbol{e}_3^\top \boldsymbol{\omega}_A$ *determined from* (6)
  return $[\boldsymbol{R}_{\text{est}}, \boldsymbol{R}_C, \alpha_0]$
end procedure

Proposition IV.1. *$\boldsymbol{R}_{\tilde{\boldsymbol{v}}\to\boldsymbol{v}}$ can be approximated as $\boldsymbol{I}_3$ if $||\Delta\boldsymbol{v}|| \ll 1$.*

Proof: Based on the discussion in Subsection III-B, we have already demonstrated that for rotating $\tilde{\boldsymbol{v}} = \frac{\boldsymbol{v}+\Delta\boldsymbol{v}}{||\boldsymbol{v}+\Delta\boldsymbol{v}||} \in S^2$ to $\boldsymbol{v} \in S^2$, if the angle of separation is θ, then $\cos\theta = \frac{\boldsymbol{v}^\top(\boldsymbol{v}+\Delta\boldsymbol{v})}{||\boldsymbol{v}+\Delta\boldsymbol{v}||} = \frac{1+\boldsymbol{v}^\top\Delta\boldsymbol{v}}{||\boldsymbol{v}+\Delta\boldsymbol{v}||}$. If we define $\cos\phi = \frac{\Delta\boldsymbol{v}^\top\boldsymbol{v}}{||\Delta\boldsymbol{v}||}$, $\cos\theta = \frac{1+||\Delta\boldsymbol{v}||\cos\phi}{||\boldsymbol{v}+\Delta\boldsymbol{v}||} = \frac{1+||\Delta\boldsymbol{v}||\cos\phi}{\sqrt{1+||\Delta\boldsymbol{v}||^2+2||\Delta\boldsymbol{v}||\cos\phi}}$.

For $||\Delta\boldsymbol{v}|| \ll 1$, $\cos\theta \approx 1 \Rightarrow \boldsymbol{R}_{\tilde{\boldsymbol{v}}\to\boldsymbol{v}} \approx \boldsymbol{I}_3$. ■

Since $\Delta\boldsymbol{v}$ is generally unknown, Proposition IV.1 provide conditions under which the estimator described in (5) is valid. This proposition suggests that accelerometers can be used as the vector correspondence when the body experiences low accelerations.

C. Error analysis for the estimation of $\dot{\boldsymbol{v}}$ and $\boldsymbol{R}_A$

We use $\dot{\boldsymbol{r}}_i = \boldsymbol{\omega} \times \boldsymbol{r}_i$ to estimate the derivative of a vector $\boldsymbol{v} \in S^2$. The first-order error in this estimate in the presence of additive noise is $\Delta\dot{\boldsymbol{v}} = \Delta\boldsymbol{v} \times \boldsymbol{\omega} + \boldsymbol{v} \times \Delta\boldsymbol{\omega}$. This error in the estimate is independent of sampling frequency and depends only on the measurement noise.

The numerical integration for estimation of $\boldsymbol{R}_A$ is done using the Euler's method of integration of (6). If we define h as the sampling time period, then this method of integration has an error of estimate in the order of $\mathcal{O}(h^2)$.

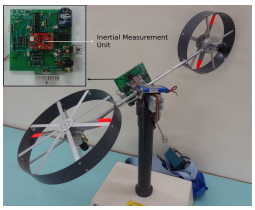

(a) TRMS

(b) Spherical Robot

Figure 3: Experimental setups

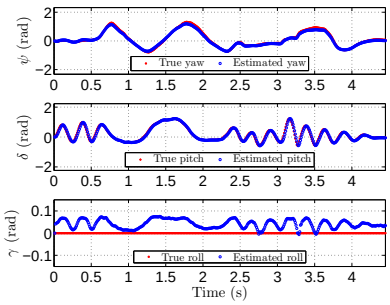

Figure 4: TRMS Euler angles (ψ, δ, γ) - Iteration 1 in Table II

V. Experimental Validation

The proposed algorithm is tested on two laboratory setups - Twin Rotor MIMO system (TRMS) and spherical robot. While TRMS is analyzed for the accuracy of the reduced attitude estimate, the spherical robot is used for rigorous validation of the repeatability and global validity of the attitude estimate.

A. Twin Rotor MIMO System

The Twin Rotor MIMO system from Feedback™, shown in Figure 3a, has 2-DOF namely, yaw and pitch motion. The roll motion is absent. An IMU is mounted on the pivot of the system such that it experiences minimal linear acceleration. The accelerometer readings, therefore, can be approximated as the true resolution of gravity in the body frame $\{\mathbb{G}\}$. The IMU used for this experiment is a low-cost Sparkfun 9 Degrees-of-Freedom - Razor IMU (SEN-10736). The signals are filtered in order eliminate high frequency noise.

The objective here is to estimate the yaw and pitch of the TRMS and establish the accuracy of the reduced attitude estimate.

Experiments on TRMS: The framework described in Subsection III-A is used for the experimental validation with $\boldsymbol{R}_I = \boldsymbol{I}_3$ and $\boldsymbol{R}_B = \boldsymbol{R}_{\boldsymbol{e}_2'}(\frac{\pi}{2})$. Due to zero-roll dynamics, α_0 is the yaw angle in ZYX representation. The estimate for $\dot{\alpha}_0$ and $\boldsymbol{R}_V$ form the reduced attitude estimate for the system as discussed in Subsection III-E.

The true value for yaw and pitch are obtained from incremental encoders and is compared with the estimates provided by DAESR which is presented in Figure 4. It should be noted that the estimate for yaw is obtained by numerically integrating the estimate of $\dot{\alpha}_0$ from (6). The repeatability of the estimator can be seen in Table II.

Iteration	Maximum Absolute (radian)		RMS Error (radian)		Correlation %	
	Yaw	Pitch	Yaw	Pitch	Yaw	Pitch
1	0.1330	0.1157	0.0627	0.0011	99.53	99.66
2	0.1869	0.1740	0.0620	0.0011	99.40	98.92
3	0.1775	0.0993	0.0838	0.0015	99.23	99.53
4	0.1805	0.1316	0.0737	0.0013	99.66	99.51
5	0.1389	0.1497	0.0684	0.0012	99.06	99.17

Table II: Errors in estimated yaw and pitch in TRMS

True roll is assumed to be zero in Figure 4 because the platform on which the TRMS experiment is presumed to be on a plane orthogonal to the gravity. From Proposition III.1 and Subsection III-E, we conclude $\gamma = \text{atan2}(a_y, a_z)$ which means body acceleration picked up by the accelerometer also affects the roll estimate. The accurate estimation of yaw and pitch, in the presence of low linear accelerations and experimental inadequacies, is an indicator of the robustness of DAESR in reduced attitude estimation.

B. Spherical Robot

The spherical robot developed at the Dynamics and Control Lab, IIT Madras is shown in Figure 3b. It is a 5-DOF system with two translational (x, y) and 3-D rotational DOF $(\boldsymbol{R})$. The hardware is enclosed in a spherical acrylic shell composed of two detachable hemispheres. It is supported on an endoskeleton consisting of three orthogonal rings and a crossbeam. The crossbeam is used to place the IMU, Analog Devices ADIS16400, at the center of the robot.

The objective here is to estimate the attitude of the spherical robot and establish global coverage of $SO(3)$ manifold.

Experiments on spherical robot: The spherical robot is rolled on two paths - *circle* and *trifolium*. The DAESR attitude estimate is compared with the TRIAD algorithm as a standalone algorithm and as inputs to the passive complementary filter proposed in [9], denoted by DAESR+CF and TRIAD+CF respectively. The passive complementary filter is implemented without bias correction and the optimal algorithm gain k_P was chosen as 0.05 by tuning for TRIAD as the measured estimate of attitude.

The position dead-reckoning of circle and trifolium, using the non-holonomic constraints ($\dot{x} = r\boldsymbol{e}_2^\top \boldsymbol{R}\boldsymbol{\omega}$ and $\dot{y} = -r\boldsymbol{e}_1^\top \boldsymbol{R}\boldsymbol{\omega}$) can be seen in Figures 5a and 5b where r is the radius of the sphere. The performance of the algorithms are found to be similar in both the paths. Hence, for brevity, trifolium is omitted from further analysis. Three figures of merit are analyzed for the circle experiment:

1) Error in the position (x, y) dead reckoning, which involves integration of the attitude estimate. Since the radius of the circular path is fixed (1.25m), the error is defined as $|\sqrt{(x-1.25)^2 + y^2} - 1.25|$.

2) Rotational offset ($\theta_{\text{err}} \in S^1$) between attitude estimates $\boldsymbol{R}_1$ & $\boldsymbol{R}_2$,

$$1 - \cos\theta_{\text{err}} = 1 - \frac{\text{tr}(\boldsymbol{R}_1^\top \boldsymbol{R}_2) - 1}{2} = \frac{3 - \text{tr}(\boldsymbol{R}_1^\top \boldsymbol{R}_2)}{2}$$

For the experimental validation, $\boldsymbol{R}_2$ was fixed as the estimate from DAESR and the estimate from the passive complementary filter with DAESR as the measured estimate of attitude.

3) Error in the estimated body angular velocity $||(\boldsymbol{R}_1^\top \dot{\boldsymbol{R}}_1)^\vee - \boldsymbol{\omega}||$.

The results of the circle experiment are presented in Table III. Due to the presence of magnetic biases in the spherical robot setup, the position estimate has a drift when evaluated using TRIAD algorithm as seen in the Figures 5a and 5b. The claim of superiority of optimal over deterministic algorithms is justified in Figure 5c. When DAESR is used as the measured attitude estimate for the complementary filter, the dead-reckoning was found to be most accurate. Minimal error in various error measures occurs with DAESR/DAESR+CF in majority of iterations as seen in Table III. Apart from this, DAESR/DAESR+CF consistently achieves minimal RMS deviation in the integral and differential error. In iterations where the error observed in DAESR/DAESR+CF is not minimal, the deviation is found to be very small. Since the actual attitude information is unavailable, the scalar error is relative among all the algorithms and hence no minimal claim can be made. Thus, Table III shows DAESR/DAESR+CF outperforms TRIAD/TRIAD+CF in performance with lesser sensor information. The performance of DAESR/DAESR+CF also validates the choice of θ_t and the claim of global coverage of $SO(3)$ manifold.

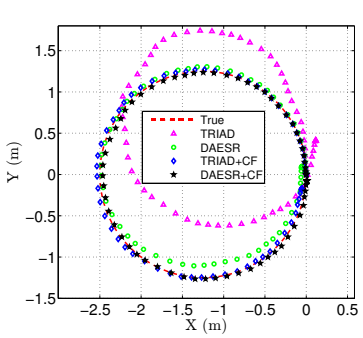

(a) Spherical robot dead-reckoning on a circular path. (Iteration 1 in Table III)

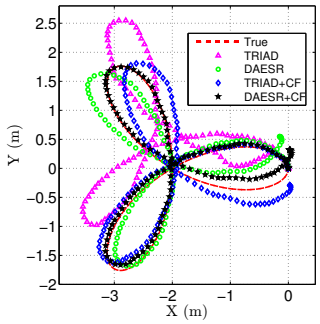

(b) Spherical robot dead-reckoning on a trifolium path.

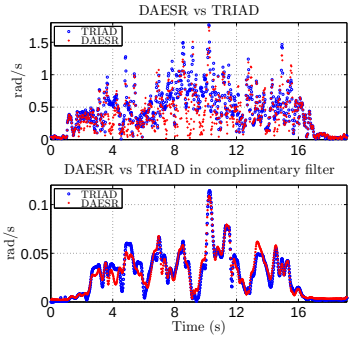

(c) $||(\boldsymbol{R}_{\text{est}}^{\top}\dot{\boldsymbol{R}}_{\text{est}})^{\vee} - \boldsymbol{\omega}||$ Spherical robot on circular path. (Iteration 1 in Table III)

Figure 5: Experimental results on spherical robot. CF denotes the complementary filter.

Iteration	Algorithm	Integral Error $\lvert\sqrt{(x-1.25)^2+y^2}-1.25\rvert$			Differential Error $\lvert\lvert(\boldsymbol{R}_{\text{est}}^{\top}\dot{\boldsymbol{R}}_{\text{est}})^{\vee}-\boldsymbol{\omega}\rvert\rvert$		Scalar Error $\frac{\lvert 3-\text{tr}(\boldsymbol{R}_{\text{est}}^{\top}\boldsymbol{R}_{D})\rvert}{2}$		$\frac{\lvert 3-\text{tr}(\boldsymbol{R}_{\text{est}}^{\top}\boldsymbol{R}_{DO})\rvert}{2}$	
		MAE (m)	RMSE (m)	Final Offset (m)	MAE (radian/s)	RMSE (radian/s)	MAE	RMSE	MAE	RMSE
1	TRIAD	0.7425	0.4213	0.4293	1.804	0.533	0.1402	0.0315	0.2124	0.0530
	DAESR	0.3582	0.2357	0.1218	1.765	0.463	0	0	0.0274	0.0089
	TRIAD+CF	0.3000	0.2516	0.1787	0.155	0.075	0.0247	0.0097	0.0032	0.0020
	DAESR+CF	0.2847	0.2501	0.0970	0.159	0.075	0.0274	0.0089	0	0
2	TRIAD	0.4019	0.2992	0.3896	6.591	1.115	0.5848	0.1567	0.2489	0.0709
	DAESR	0.5811	0.3082	0.6067	6.956	1.125	0	0	0.1299	0.0289
	TRIAD+CF	0.3533	0.2891	0.2580	0.317	0.073	0.2242	0.0921	0.0603	0.0271
	DAESR+CF	0.3004	0.2245	0.2370	0.316	0.074	0.1299	0.0289	0	0
3	TRIAD	0.4854	0.3015	0.4008	6.894	0.979	0.3867	0.0978	0.3339	0.0719
	DAESR	0.2557	0.1807	0.4566	8.006	1.023	0	0	0.0479	0.0122
	TRIAD+CF	0.2906	0.2463	0.1384	0.318	0.057	0.1231	0.0458	0.0267	0.0122
	DAESR+CF	0.2903	0.2142	0.1427	0.319	0.057	0.0479	0.0122	0	0
4	TRIAD	0.5355	0.3048	0.0858	3.798	0.853	0.2424	0.0720	0.2514	0.0773
	DAESR	0.3677	0.2459	0.1238	5.454	0.836	0	0	0.0345	0.0028
	TRIAD+CF	0.2718	0.2357	0.1053	0.260	0.055	0.0317	0.0108	0.0263	0.0107
	DAESR+CF	0.2762	0.2134	0.1293	0.258	0.053	0.0345	0.0028	0	0
5	TRIAD	0.5855	0.3471	0.2215	5.689	0.890	0.2228	0.0516	0.2420	0.0629
	DAESR	0.2878	0.2100	0.1258	5.291	0.787	0	0	0.0178	0.0029
	TRIAD+CF	0.2591	0.2131	0.0366	0.238	0.051	0.0237	0.0056	0.0106	0.0058
	DAESR+CF	0.2765	0.2056	0.0992	0.234	0.049	0.0178	0.0029	0	0

MAE - Maximum Absolute Error, RMSE - Root Mean Square Error, $\boldsymbol{R}_D$ - Attitude estimation from DAESR,
CF - Complementary Filter, $\boldsymbol{R}_{DO}$ - Attitude estimation using DAESR as the measured estimate of attitude for CF.

Table III: Robustness analysis of attitude estimation - spherical robot rolling on a circular path. The minimum error in each of the error measure is marked for every iteration. Video demonstration of the Iteration 1 can be found at http://youtu.be/ounyQH_W2os.

VI. Conclusion

We have presented an attitude estimator for a rigid body using a single vector information and rate gyros. The DAESR algorithm was validated through experiments. The advantages of DAESR over other algorithms, revealed from the spherical robot experiment, are attitude passing through the entirety of $SO(3)$ is estimated and the position obtained from two-level integration has negligible drift. Relaxing the restrictions on constant $\boldsymbol{v}_e$ and linear accelerations is a future pursuit.

References

[1] R. N. Murray, Z. Li, and S. Sastry, *A Mathematical Introduction to Robotics Manipulation*, 1st ed. CRC Press, 1994.

[2] T. Lee, M. Leok, and N. H. McClamroch, "Geometric tracking control of a Quadrotor UAV on SE(3)," *49th IEEE Conference on Decision and Control (CDC), Atlanta, GA*, pp. 5420–5425, 2010.

[3] N. Madinehi, "Rigid body attitude estimation: An overview and comparative study," *University of Western Ontario - Electronic Thesis and Dissertation Repository. Paper 1259*, 2013.

[4] F. Aghili and A. Salerno, "Driftless 3-D attitude determination and positioning of mobile robots by integration of IMU with two RTK GPSs," *IEEE/ASME Transactions on Mechatronics*, vol. 18, pp. 21–31, 2013.

[5] S. Shen, Y. Mulgaonkar, N. Michael, and V. Kumar, "Vision-based state estimation for autonomous rotorcraft MAVs in complex environments," *International Conference on Robotics and Automation, Germany*, 2013.

[6] J. R. Wertz, *Spacecraft Attitude Determination and Control*. Kluwer Academic Publishers, Dordrecht, 1978.

[7] M. Shuster, "Deterministic three-axis attitude determination," *The Journal of the Astronautical Sciences*, vol. 52, no. 3, pp. 405–419, 2004.

[8] G. Wahba, "A least squares estimate of satellite attitude," *SIAM Review*, vol. 7, no. 3, p. 409, 1965.

[9] R. Mahony, T. Hamel, and J.-M. Pflimlin, "Nonlinear complementary filters on the special orthogonal group," *IEEE Transactions on Automatic Control*, vol. 53, no. 5, pp. 1203–1218, June 2008.

[10] M. D. Shuster, "In quest of better attitudes," *Advances in the Astronautical Sciences*, vol. 108, pp. 2089–2117, 2001.

[11] Black, "A passive system for determining the attitude of a satellite," *American Institute of Aeronautics and Astronautics (AIAA) Journal*, vol. 2, no. 7, pp. 1350–1351, 1964.

[12] W. Premerlani and P. Bizard, "Direction cosine matrix IMU: Theory," May, 2009. [Online]. Available: gentlenav.googlecode.com/files/DCMDraft2.pdf

[13] G. Piovan and F. Bullo, "On coordinate-free rotation decomposition: Euler angles about arbitrary axes," *IEEE Transactions on Robotics*, vol. 28, no. 3, pp. 728–733, 2012.

[14] M. D. Shuster and S. D. Oh, "Three-axis attitude determination from vector observations," *Journal of Guidance and Control*, vol. 4, no. 1,

pp. 70–77, January-February 1981.
[15] Press *et al.*, *Numerical Recipes - The Art of Scientific Computing*, 3rd ed. Cambridge Press, 2007.
[16] M. Shuster, "Survey of attitude representations," *The Journal of the Astronautical Sciences*, vol. 41, no. 4, pp. 439–517, January 1981.
[17] V. Muralidharan and A. Mahindrakar, "Position stabilization and waypoint tracking control of mobile inverted pendulum robot," *IEEE Transactions on Control Systems Technology*, 2014.
[18] N. A. Chaturvedi, A. K. Sanyal, and N. H. McClamroch, "Rigid-body attitude control," *IEEE Control Systems Magazine*, pp. 30–51, June 2011.
[19] M. Grewal and A. Andrews, "How good is your gyro?" *IEEE Control Systems Magazine*, vol. 30, no. 1, pp. 12–86, 2010.